

CONFERENCES AND SYMPOSIA

PACS numbers: **01.10.–m**, 01.10.Fv, **12.20.–m**, 41.75.Jv, **42.25.–p**, **42.62.–b**, 42.65.Re, **52.35.–g**, 52.38.Kd, 52.50.Jm, 52.65.Rr, 87.57.*uh*

Ultrastrong light fields
(Scientific session of the Physical Sciences Division of the Russian Academy of Sciences, 29 October 2014)

DOI: 10.3367/UFNe.0185.201501e.0077

On 29 October 2014, the scientific session "Super strong light fields" of the Physical Sciences Division (PSD), Russian Academy of Sciences (RAS), was held at the conference hall of the Lebedev Physical Institute, RAS.

The agenda of the session announced on the website www.gpad.ac.ru of the PSD RAS contains the reports:

(1) **Bychenkov V Yu** (Lebedev Physical Institute, RAS, Moscow) "Laser acceleration of ions: New results and prospects for applications";

(2) **Kostyukov I Yu** (Institute of Applied Physics, RAS, Nizhnii Novgorod) "Plasma methods for electron acceleration: the state of the art and outlook";

(3) **Zheltikov A M** (Lomonosov Moscow State University, Moscow) "Nonlinear optics of mid-IR ultrashort pulses";

(4) **Narozhnyi N B, Fedotov A M** (Moscow Engineering Physics Institute, Nuclear Research University, Moscow) "Quantum electrodynamics cascades in intense laser fields."

Papers written on the basis of oral presentations 1–4 are published below.

PACS numbers: 52.38.Kd, 52.50.Jm, 52.65.Rr, *87.57.uh*
DOI: 10.3367/UFNe.0185.201501f.0077

Laser acceleration of ions: recent results and prospects for applications

V Yu Bychenkov, A V Brantov, E A Govras, V F Kovalev

Abstract. **We present a brief review of recent theoretical and numerical simulation results on the acceleration of ions from various targets irradiated by high-power femtosecond laser pulses. The results include: the optimization of the laser–plasma acceleration of ions over the thickness of a solid target; a new dependence of the energy of accelerated protons from a semitransparent foil on the incident pulse energy; a theoretical model of plasma layer expansion in the vacuum for a fixed temperature of heated electrons, describing arbitrary regimes of particle acceleration, from the quasineutral flow of a plasma to Coulomb explosion; analytic theories of the relativistic Coulomb explosion of a spherical microtarget and the radial ponderomotive acceleration of ions from a laser channel in a transparent plasma; and calculations optimizing the production of isotopes for medicine using next-generation lasers.**

Uspekhi Fizicheskikh Nauk **185** (1) 77 – 110 (2015)
DOI: 10.3367/UFNr.0185.201501e.0077
Translated by M Sapozhnikov, A L Chekhov, A M Zheltikov, E G Strel'chenko; edited by A M Semikhatov, A Radzig

Keywords: laser pulse, target, particle acceleration, laser channel, plasma expansion, Coulomb explosion, isotope production

1. Introduction

Laser methods for accelerating charged particles to high energies became dominant in the high-energy-density laser physics immediately after the advent of multiterawatt femtosecond and subpicosecond lasers at the end of the 20th century. While the energy of laser-accelerated electrons has been continuously increasing in recent years and changed from a few MeV to a few GeV in a decade, quite a different situation is observed for ions (mainly protons), whose energy has not exceeded 70 MeV per nucleon according to the literature [1]. At first glance, it is difficult to speak about any considerable progress in laser-induced acceleration of heavy particles, because one of the first results, $\varepsilon \approx 58$ MeV [2], obtained for accelerated protons fifteen years ago, is formally close to modern achievements [1]. However, taking into account that the result in [2] was obtained for a 400 J pulse, while that in [1] was for a 80 J pulse, the progress is obvious, although not so impressive as for the laser acceleration of electrons.

Unlike laser energy conversion to acceleration of electrons, laser energy conversion to acceleration of ions first involves the electron energy conversion to the quasi-static energy of the field and then the transformation of the latter into the ion energy. Obviously, such a longer laser energy transformation chain (laser–electrons–field–ions) is not very efficient, and producing ion beams with the maximum energy and the maximum number of particles requires the appropriate optimization. An important stage in the search for ways to increase the ion acceleration efficiency was the discovery of the increase in the maximum energy of ions upon decreasing the target thickness, which was distinctly observed in experiments with laser pulses having a high intensity contrast [3–6]. This allowed avoiding premature damage of the target before the main pulse arrived. True, the required preservation of an ultrathin target has not been achieved so far, because the pulse intensity contrast is still insufficient, even if increased by many orders of magnitude over that achieved previously using a double plasma mirror [7]. Nevertheless, the radical improvement in

V Yu Bychenkov, A V Brantov, E A Govras, V F Kovalev
Lebedev Physical Institute, RAS, Moscow, Russian Federation;
Center for Fundamental and Applied Studies, Dukhov All-Russian Research Institute of Automatics, Moscow, Russian Federation
E-mail: bychenkov@lebedev.ru

Uspekhi Fizicheskikh Nauk **184** (1) 77 – 88 (2015)
DOI: 10.3367/UFNr.0185.201501f.0077
Translated by M Sapozhnikov; edited by A M Semikhatov

the pulse quality has already provided a quite accurate determination of the required target thicknesses for multi-joule femtosecond laser pulses and has given a promising result on the generation of 21 MeV protons by a 3 J laser pulse with an energy a few orders of magnitude lower than that of record laser pulses used for ion acceleration.

Thin targets allow the heating and acceleration of electrons in a focal spot over the entire thickness of a foil. Electrons escaping from this volume of the target release the Coulomb energy of the volume, which is spent to accelerate ions. This energy is maximal for the target thickness determined by the balance of the Coulomb and laser fields, $E_C = E_{las}$, because otherwise either the laser field is too weak to remove electrons from the foil or the number of electrons is too small because the foil thickness l is not large enough, which follows from the relation $E_C \propto l$. This condition gives $l = l_{opt} \approx a_0(\lambda/\pi)\, n_c/n_e$, where n_e is the electron density in the plasma, $n_c = m_e/(4\pi e^2\omega^2)$ is the critical plasma density, and $a_0 = 0.85\,\{I\,[\mathrm{W\,cm^{-2}}]\,(\lambda\,[\mu\mathrm{m}])^2\,10^{-18}\}^{1/2}$ is the standard dimensionless laser field amplitude with the wavelength λ. It is easy to verify that this condition determines the relativistic transparency threshold for plasma [8], which ensures the presence of the laser field everywhere inside the target and its semitransparency. Because electrons are mainly ejected to the rear of the target, the ion acceleration should be treated as a directional Coulomb explosion [11]. Obviously, the optimal target thickness l_{opt} presented above, determined from qualitative considerations, should be quantitatively refined, as is done in the case of a simplified two-dimensional numerical particle-in-cell (PIC) model [9]. In this paper, we present the results of such studies based on three-dimensional PIC simulations and also consider the corresponding simplified model describing the dependence of the maximum ion energy on the laser and plasma target parameters [10].

Most of the current studies on the acceleration of ions by femtosecond and subpicosecond laser pulses assume the use of thin planar solid targets (foils), which are the simplest to construct (as compared, for example, with a complex target [1]) and permit a rather simple optimization with respect to the specified laser pulse parameters. The laser acceleration of ions from such targets (primarily protons and deuterons) has attracted considerable interest because ion beams are promising for applications in controlled nuclear fusion [12, 13], nuclear physics [14], radiography [15, 16], nuclear pharmacology [17, 18], and hadron and neutron therapy [19, 20]. With two examples in Section 4, we demonstrate the possibilities of the optimal scheme for laser production of medical isotopes by using thin solid targets irradiated by a new-generation laser, which was discussed within the ICAN (International Coherent Amplification Network) project [21].

Of course, modern three-dimensional kinetic codes allow simulating the acceleration of particles during the interaction of short laser pulses with various targets. However, because numerical calculations consume a great amount of resources and contain multiparametric dependences, they must be verified by theoretical models. The scarcity of such models in high-energy physics restrains the development of new optimal schemes for laser acceleration of ions. The aim of such theoretical models, even if they are rather simplified, is to reveal characteristic dependences of the acceleration of particles on the target parameters and to outline the region of these parameters providing the best quality of the beam, as well as to propose new acceleration schemes and to estimate possible effects for next-generation laser schemes. In this connection, we include analytic theories of ion acceleration from a gas plasma and a cluster in this review.

2. Optimization of a laser–plasma source of high-energy ions

The search for optimal targets for different laser acceleration regimes of ions is a key problem [22]. The interaction of high-power short laser pulses with matter is a complex nonlinear process. We simulate this process using the three-dimensional completely relativistic Mandor code [23] for solving the system of Maxwell–Vlasov equations by the PIC method.

2.1 Numerical simulation

To determine the optimal thickness of a solid foil target, we perform a series of three-dimensional calculations of proton acceleration by ultrashort 30 fs laser pulses focused onto a spot with the diameter $d = 4\lambda$ measured at the laser beam intensity half-width. Without losing the generality of the results obtained, we assume that the laser wavelength is $\lambda = 1$ μm. The maximum laser radiation intensity I on the target ranges from 5×10^{18} to 5×10^{22} W cm^{-2}, corresponding to a change in the laser pulse energy from 0.03 to 300 J.

To analyze the influence of the focal spot diameter d on proton acceleration, we performed calculations for a tightly focused laser beam near the diffraction limit ($d = 2$ μm). Such a focusing is described with the help of exact electromagnetic fields corresponding to focusing with a parabolic mirror. For larger spots, Gaussian beams are used. A laser pulse is focused on the front side of thin plasma (CH_2) targets consisting of electrons, protons, and completely ionized carbon atoms (C^{6+}). The electron density in the target is $200\,n_c$, corresponding to the solid mass density of CH_2 equal to 1.1 g cm^{-3}. For each level of laser radiation intensity, the target thickness is varied near the predicted theoretical optimal value l_{opt} in the range from 3 nm to 1 μm.

As mentioned above, the maximum proton energy as a function of the target thickness and laser energy obtained from simulations (Fig. 1) shows the existence of an optimal target thickness. The optimal target thickness linearly increases with increasing the laser field amplitude, $l_{opt} = 0.5\lambda a_0 n_c/n_e$, where the numerical coefficient 0.5, almost independent of the focal spot size, is somewhat larger than

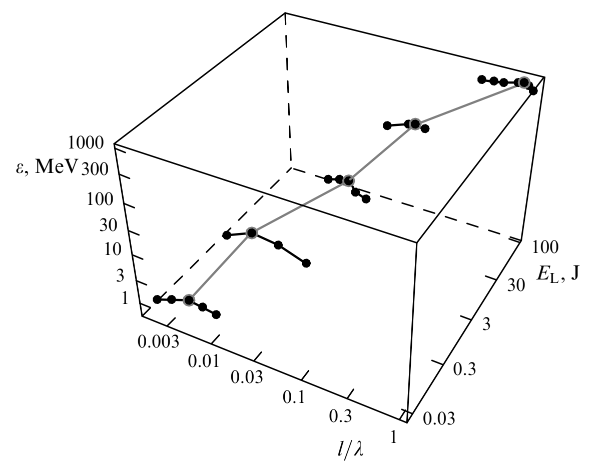

Figure 1. Dependence of the maximum proton energy ε on the target thickness l and the laser energy E_L for $d = 4$ μm.

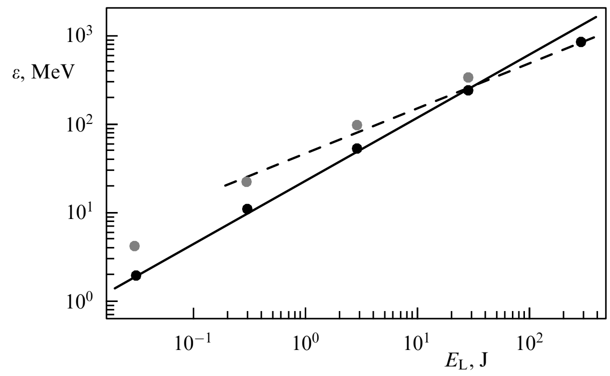

Figure 2. Dependences of the maximum proton energy on the laser energy for the optimal target thickness and $d = 4$ μm (dark dots) and $d = 2$ μm (light dots). The solid and dashed straight lines correspond to scalings $\varepsilon\,[\mathrm{MeV}] = 22\,(E_L\,[\mathrm{J}])^{0.7}$ and $\varepsilon\,[\mathrm{MeV}] = 45\,(E_L\,[\mathrm{J}])^{0.5}$ [9].

the predicted theoretical value $1/\pi$ [8]. A target with the optimal thickness is partially transparent to laser light, and hence the electrons in the focal volume are heated virtually uniformly and are ejected from plasma forward, producing a strong charge-separating field [24]. The ions are accelerated in this field as in a directional Coulomb explosion [11]. Upon removing a large number of electrons from the focal region, the laser pulse can penetrate still deeper, and because laser pulses can efficiently heat thick targets, the obtained optimal thickness somewhat exceeds its theoretical value.

Figure 2 shows the dependence of the maximum proton energy on the laser pulse energy. The simulation results are well approximated by the power scaling as $\varepsilon_{\max} \propto E_L^{0.7}$, which differs from the root dependence proposed earlier [9]. For the specified laser pulse energy, the tighter focusing leads to an increase in the maximum energy of protons. The number of fast particles increases with increasing the laser energy.

To clarify the nature of the obtained proton energy scaling, we analyze the absorption of laser light in semi-transparent targets. We define the absorption coefficient A as the ratio of the total kinetic energy of all particles to the initial laser energy. For our parameters, the energy absorption coefficient of targets with the optimal thickness for 30 fs pulses increases with the laser energy from 10% for a 0.03 J laser to 30% for a 30 J laser and is determined by the relation $A = 0.15\,E_L^{\beta}$, where $\beta \sim 0.2$. Because the energy of accelerated ions is proportional to the characteristic electron energy, which in turn increases as a function of the absorbed laser energy, the dependence of ε on E_L becomes stronger than the dependence $\varepsilon_{\max} \propto E_L^{0.5}$ corresponding to the usual ponderomotive scaling [28] that neglects the increase in the absorption coefficient upon optimization of the target thickness.

2.2 Theoretical model

In this section, we show how a simple semianalytic theory can qualitatively describe the results of complicated simulations for determining the maximum possible energy of accelerated ions from thin planar targets. We assume that the plasma has a thickness l along the x axis. The transverse size of the plasma is restricted by the laser focal spot $\pi d^2/4$. For simplicity, we consider plasma with ions of one species, which are initially at rest in the region $-l/2 < x < l/2$. During the subsequent motion of ions, plasma electrons, remaining in equilibrium with the electrostatic field, are described by the Boltzmann distribution with the effective temperature T_e: $n_e(x,t) = n_{e0}\exp\left(e\,\varphi(x,t)/T_e\right)$, where n_{e0} is the initial electron density at the foil center. The electron temperature depends on the laser intensity and can also depend on time due to the adiabatic cooling of electrons after the laser pulse is switched off. The plasma expansion for $t > 0$ is symmetric with respect to the $x = 0$ plane. At small distances $x_f < d$, where $x_f(t)$ is the ion front position, three-dimensional effects are insignificant because of the finite transverse size of the plasma, and the plasma expansion can be considered one-dimensional. The motion of plasma ions in this case is described by the system of equations

$$
\begin{aligned}
&\varphi'' = 4\pi\left(e\,n_e(x,t) - Zen_i(x,t)\right),\\
&\varphi'\big|_{x=0} = 0\,, \quad \varphi'\big|_{x=\infty} = 0\,,\\
&M\ddot{x} = -Ze\,\frac{\partial\varphi}{\partial x}\,, \quad \dot{x}(0) = 0\,,\\
&x(0) = x_0\,, \quad 0 \leqslant x_0 \leqslant \frac{l}{2}\,,\\
&n_i(x,t) = n_0\left|\frac{\partial x}{\partial x_0}\right|^{-1}.
\end{aligned}
\tag{1}
$$

We introduce dimensionless variables such that the spatial coordinate x is measured in units of $l/2$, time t is normalized to $1/\omega_{pi}$, densities n_i and n_e are normalized to n_0, and energies ZT_e and $Ze\varphi$ are expressed in units of $4\pi\,(Ze)^2\,n_0\,(l/2)^2$. The density n_{e0}, which is determined by the initial ion density n_0 and the ion charge Z, depends on the initial temperature approximately as $n_{e0} = Zn_0(1 + 2\,T_{e0})^{-1}$ [25]. At present, analytic solutions of system (1) are found only in the case $\lambda_{De} \ll l$, i.e., for a quasilinear plasma expansion, $T_e \to 0$, [26] and in the case of Coulomb explosion $\lambda_{De} \gg l$, $T_e \to \infty$ [27]. For a quasilinear expansion, $n_i \approx n_e$ and the electric field on the ion front has the form $E_l = 2(T_e)^{1/2}/(2\mathrm{e} + t^2)^{1/2}$ [26], where $\mathrm{e} = 2.71828\ldots$. In the opposite limit (Coulomb explosion), $n_i = 1/x_f(t)$ and $E_l \equiv 1$ [27].

To obtain an approximate solution of system (1) for an arbitrary ratio λ_{De}/l avoiding the time-consuming self-consistent calculation of the ion density, we found an interpolation relation for $n_i(x,t)$ that is valid at arbitrary temperatures T_e. It follows from the Poisson equation in (1) that $E_l = \int_0^{x_f}(n_i(x,t) - n_e(x,t))\,\mathrm{d}x$. If we set $n_i(x,t) = n_e(x,t) + E_l/x_f$, then the relation for E_l is satisfied automatically, and we obtain the correct limit transitions to the quasi-neutral expansion and Coulomb explosion regimes. Solving the Poisson equation in (1) with this ion density, we find an implicit formula for the function $E_l(x_f)$:

$$
(E_l)^{-1} = 1 + \sqrt{\frac{x_f E_l}{2T_e}}\,\exp\left(\frac{x_f E_l}{2T_e}\right)\operatorname{erf}\left(\sqrt{\frac{x_f E_l}{2T_e}}\right), \tag{2}
$$

where $\operatorname{erf}(z) = \int_0^z \exp(-t^2)\,\mathrm{d}t$. We assume that plasma electrons are heated by the laser to a characteristic temperature T_{e0} during the laser pulse action time $t < \tau$. After the laser pulse is switched off, $t > \tau$, the electrons begin to cool adiabatically, as described in [29]. The time dependence of the electron temperature in this case can be written in the form

$$
T_e(t) = T_{e0}\left[\Theta(\tau - t) + \frac{\Theta(t - \tau)}{1 + (t-\tau)^2/t_c^2}\right], \tag{3}
$$

where $\Theta(t)$ is the Heaviside function, and the characteristic cooling time is defined as $t_c = L/\sqrt{2}\,c_s$. Here, L is the characteristic spatial scale of the ion density and c_s is the ion sound speed. We choose the characteristic values $L = x_f(\tau)$ and $c_s = \sqrt{T_{e0}}$.

When the ion plasma expands over distances $x_f \sim L_1 = 1 + d$, it is necessary to take the rapid decrease in the accelerating field into account. Because of the finite volume occupied by the plasma, the accelerating field decreases $\propto x^{-2}$ for $x_f \gg L_1$. By matching the two asymptotic forms of the field at the front, E_1 in (2) for $x_f < L_1$ and $E_1(L_1)/(x - L_1)^2$ for $x_f \gg L_1$, we can propose a smooth dependence valid for any position x_f of the front. In addition, the laser pulse action introduces an asymmetry into the plasma expansion because all electrons are accelerated forward from the rear side of the target. We assume that for this reason the electric field for $x > 0$ is twice as large as E_1 in (2), obtained for the symmetric expansion of a hot plasma layer into the vacuum. Finally, the electric field at the ion plasma front at an arbitrary instant can be written in the form

$$E(x_f) = \begin{cases} 2E_1(x_f)\,, & x_f \leqslant L_1\,, \\ 2E_1(L_1)\left[1 + (x_f - L_1)^2\right]^{-1}, & x_f > L_1\,, \end{cases} \qquad (4)$$

where the time evolution of the electron temperature in Eqn (2) for E_1 is determined by expression (3). Solving the equation of motion from (1) for ions at the expanding plasma front with the electric field $E(x_f)$ given by (4), we obtain the maximum ion energy $\varepsilon_{max} = (\dot{x}_f)^2/2$ and its dependence on the pulse duration, focal spot size, and electron temperature, which is uniquely related to the laser pulse energy.

The corresponding dependences of the maximum proton energy on the focal spot diameter and pulse duration for fixed total laser energies 3 and 30 J are presented in Fig. 3. The electron temperature T_{e0} was found from the known ponderomotive scaling $T_{e0} \propto mc^2[(1 + (a_1)^2)^{1/2} - 1]$ [28], but with the heating caused by the absorbed energy, and hence a_1 is not the vacuum amplitude of the laser field $\propto E_L \propto a_0$ but the amplitude calculated from the absorbed energy, $a_1 = a_0\sqrt{A}$. Theoretical results presented in Fig. 3 are consistent with simulation results, which show (Fig. 2) that for fixed laser pulse energy and duration, defocusing reduces the ion energy despite the possibility of increasing the effective acceleration length. We see from Fig. 3 that the dependence of the final energy on the pulse duration becomes weaker with increasing the focal spot size. This is explained by the fact that the spot diameter determines the characteristic acceleration length L_1. If the acceleration time is shorter than the full laser pulse duration, the electrostatic field energy conversion to the ion energy is incomplete, because plasma expansion passes to the three-dimensional regime accompanied by a strong decrease in accelerating fields. Therefore, there exists an optimal relation between the pulse duration and the focal spot size: to achieve the most efficient conversion of laser energy to the energy of accelerated particles, the pulse duration should not exceed the characteristic acceleration time of particles (defined as the plasma expansion time at a distance of the order of the spot diameter).

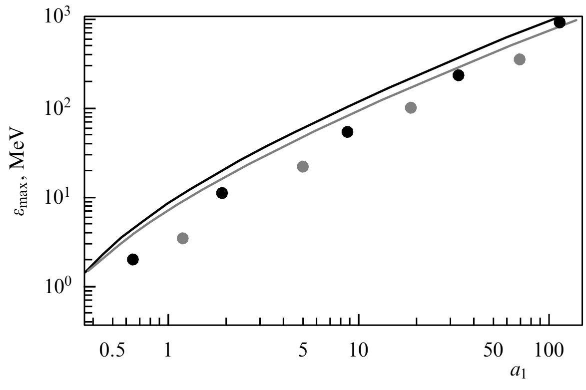

Figure 4. Maximum proton energy as a function of the amplitude a_1 of the absorbed laser field. Circles correspond to simulation results and curves are theoretical dependences. The laser parameters are $d = 2$ μm and $\tau = 30$ fs (grey dots and curves), and $d = 4$ μm and $\tau = 30$ fs (black dots and curves).

The numerically calculated (dots) and analytic (curves) maximum energies of protons from optimal-thickness targets are compared in Fig. 4. We can see that the theory correctly reproduces the dependence of the maximum energy on the laser intensity. Because we theoretically considered a one-component hydrogen target, analytic curves in Fig. 4 lie above the simulation results (up to 30% higher). This is explained by the fact that carbon ions in a two-component CH_2 target are also accelerated, spending a part of the absorbed laser pulse energy. Nevertheless, the curves in Fig. 4 demonstrate that at the qualitative level, a simple theory correctly reproduces the dependence of the proton energy on laser parameters, having a predictive power for different parameters of the laser pulse.

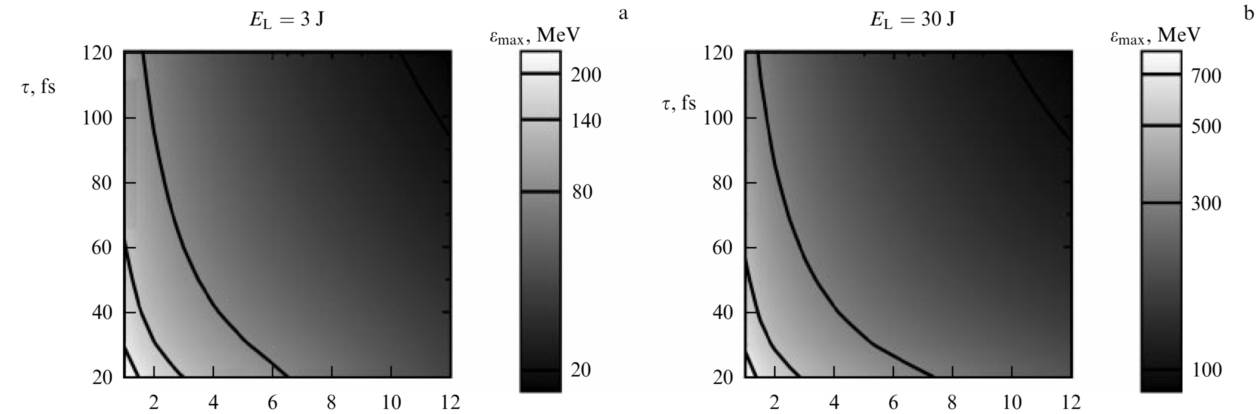

Figure 3. Maximum proton energy as a function of the focal spot diameter d and the pulse duration τ for a hydrogen foil with the density $n_e = 200n_{cr}$ and the optimal thickness l_{opt}.

3. Problem of the pulse contrast and prospects for low-density targets

The efficient acceleration of protons from ultrathin foils with the optimal thickness can be achieved due to the possibility of generating laser pulses with a high intensity contrast. Modern technologies using a double plasma mirror can provide the pulse intensity contrast up to 10^{15} on the nanosecond scale. At the same time, even comparatively weak wings on the picosecond scale can cause damage to the optimal-thickness target before the main pulse arrives [24, 30]. To estimate the influence of such a prepulse on the acceleration of ions, we simulate the behavior of a target irradiated by a laser pulse with wings, which is in fact a superposition of two Gaussian pulses: a 45 fs pulse with the peak intensity $I = 2.25 \times 10^{20}$ W cm^{-2} (the main pulse) and a 300 fs pulse with $I = 5 \times 10^{18}$ W cm^{-2} (wings); the temporal profile of the pulse is presented in the inset in Fig. 5. The target is a completely ionized plasma layer consisting of electrons, protons, and C^{+6} carbon ions. The electron density is $100n_c$ and the target thickness ranges from 20 to 100 nm.

The results of numerical experiments show that the prepulse can destroy a target with the optimal thickness of 40 nm before the main pulse arrival, resulting in a decrease in the maximum proton energy from 40 MeV (for a laser with the ideal contrast) to 30 MeV (Fig. 5), even though the prepulse additionally contains $\sim 20\%$ of the energy. This is caused by the spreading of the sharp plasma–vacuum interface on the rear side of the target, which reduces the electrostatic charge-separating field that accelerates the ions. At the same time, the relatively short prepulse under study cannot completely destroy a thicker target with a nonoptimal thickness (100 nm), and its action on such a target only leads to the appearance of a preplasma with the electron density lower than or of the order of the critical one, in which the energy of the main laser pulse is more efficiently transformed into the energy of hot electrons. In that case, the maximum proton energy reaches 37 MeV, which exceeds the 19 MeV obtained upon irradiation of the same 100 nm thick target by an ideal pulse.

Thus, our simulation shows that the complete destruction of the target typically leads to a decrease in the ion acceleration efficiency. At the same time, the appearance of a low-density plasma at the front of the target provides a more efficient acceleration of electrons and creates favorable conditions for the acceleration of ions.

Because modern technologies allow the preparation of low-density planar targets (aerogels, nanoporous materials) with the electron densities ranging from a few critical values to a few dozen critical values [31], the question arises of whether the use of such targets provides a more efficient acceleration of ions despite the finite contrast of the laser pulse. We note that there are already some examples demonstrating the advantages of using targets with a nearly critical density [32, 33]. Numerical PIC simulations have shown that the maximum proton energy can be increased upon decreasing the density of a hydrogen-containing target for a linearly polarized laser pulse in a realistic three-dimensional geometry [34].

The interaction of laser radiation with matter was simulated for a 30 fs, 3 J laser pulse focused onto a 4 μm spot on the surface of a completely ionized CH_2 target with the electron density varied from the solid-state density, equal to 200 critical densities, to 10 critical densities. Figure 6 shows the dependence of the maximum proton density on the surface density $n_e l/(n_c \lambda)$ of irradiated targets. We can see that, as before, an optimal density exists for each target, and it increases as the density decreases. In this case, the total number of electrons involved in the interaction, determined by the surface density, remains almost the same for all optimal target thicknesses. We recall that the optimal thickness of a target corresponds to a semitransparent target, which partially reflects and partially transmits a laser pulse [30]. We can see that the maximum proton energy increases with decreasing the target density. In this case, while the decrease in density from $200\,n_c$ to $20\,n_c$ leads only to a weak increase in the maximum energy from 56 to 60 MeV, a further decrease in density to $10\,n_c$ results in an increase in the proton energy by 30%, i.e., to 73 MeV.

As the target density is decreased, the higher-energy protons are ejected from the irradiated front surface of the target. These protons acquire an initial acceleration in the charge-separating field from electrons removed from the frontal surface by the ponderomotive force of the leading edge of a short light pulse and are then additionally accelerated in the charge-separating field produced by heated electrons near the rear surface of the target, as occurs in the standard ion-acceleration mechanism. If protons arrive at the rear surface of the target simultaneously with reaching

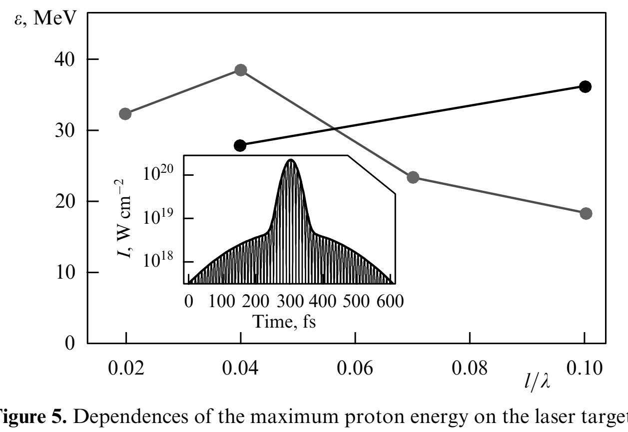

Figure 5. Dependences of the maximum proton energy on the laser target thickness irradiated by a 2 J laser pulse with the ideal contrast (grey dots) and with a complex profile of the picosecond prepulse (shown in the inset) (black dots).

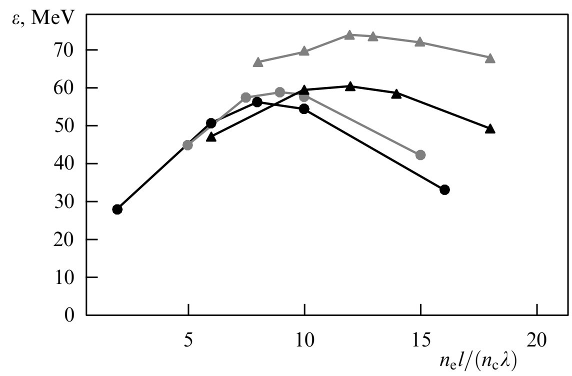

Figure 6. Dependences of the maximum proton energy on the dimensionless surface density $n_e l/(n_c \lambda)$ of the target for $200\,n_c$ (black dots), $50\,n_c$ (grey dots), $20\,n_c$ (black triangles), and $10\,n_c$ (grey triangles).

the laser pulse maximum on the target, the total acceleration of protons is the most efficient, which is realized in the case under study for targets with the density equal to $10\,n_c$.

Thus, upon synchronization of the pulse duration with the optimal target thickness, the two-stage acceleration regime, in which protons accelerated from the front surface of the target acquire the maximum energy, is the most efficient.

The possibility of increasing the energy of laser-accelerated protons by 30% by using only low-density targets is, of course, of practical interest. This is first and foremost important for using short-pulse high-power lasers to initiate nuclear reactions [14], because even a small increase in the energy of accelerated particles can lead to the initiation of new nuclear reactions because of their threshold nature. The possibility of using laser pulses for the production of isotopes in nuclear reactions is discussed in Section 4.

4. Laser-based nuclear pharmacology

One of the promising applications of laser-accelerated ion beams is their use to initiate nuclear reactions [14]. The possibility of generating directional neutron beams [35] and the production of short-lived isotopes [17] required for nuclear medicine, for example, is being widely discussed. At present, some radioactive isotopes for medicine are produced in nuclear reactors. For example, the leading world suppliers of technetium-99m, the most widely used isotope in nuclear medicine (up to 80% of all diagnostic procedures) are two reactors in Canada and the Netherlands, which are planned for closing in the coming years [36]. In this connection, the search is underway for new methods for producing this technetium isotope, notably, using proton beams in cyclotrons [37]. The development of modern laser technologies, in particular, the creation of a laser with a high mean power [21], will allow the efficient application of laser-accelerated protons in medicine [18]. Ion beams (usually proton or deuteron beams) obtained by laser methods can be efficiently used to produce isotopes for single-photon emission computer tomography (SPECT) (Tc-99m), for positron-emission tomography (PET) (for example, the carbon isotope C-11), and for obtaining neutron beams used in medicine for boron-capture therapy and fast-neutron therapy, like using beams in hadron therapy [38].

As in Section 2, the optimal thickness of the target (thin plastic CH_2/CD_2 films) is determined to obtain the maximum number of protons/deuterons to increase the yield of isotopes and neutrons from the second target irradiated by laser-accelerated particles. To obtain the optimal parameters of the ion beam, we performed three-dimensional calculations of the action of a high-power 10 J, 100 fs linearly polarized laser pulse on ultrathin planar CH_2 or CD_2 targets. The chosen laser parameters correspond to those of a new-generation 10 kHz laser proposed within the ICAN project [21]. We also performed calculations for 5 J and 1 J laser pulses.

A 1 μm laser pulse was focused onto a 4 μm spot on the front surface of a target. For a 10 J laser, focusing onto 6 μm and 10 μm spots was also considered, while a 1 J laser pulse was focused only onto a 2 μm size. The target consisted of electrons, completely ionized carbon ions, and protons (or deuterons). The electron density $200n_c$ approximately corresponded to the real density of a completely ionized plastic target ($1.1\ \mathrm{g\,cm^{-3}}$). By varying the target thickness from 20 nm to 0.5 μm, we obtained the dependences of the maximum proton energy and the number of energetic protons on the target thickness (Fig. 7) for different irradiation conditions (different focal spot sizes). As shown above, the optimal interaction regime corresponds to semitransparent targets with the thickness determined by the initial electron density and maximum laser intensity. For example, the tight focusing of a 1 J laser pulse onto a 2 μm spot produces approximately the same intensity on the target as the focusing of a 5 J laser pulse onto a 4 μm laser spot, and therefore the optimal target thickness is the same in both cases.

To initiate nuclear reactions, it is necessary to obtain the maximum number of protons/deuterons with the energy exceeding the threshold (for example, above 8 MeV for the Mo-100(p, 2n)Tc-99m reaction). In general, the number of accelerated particles increases with the focal spot size and the laser pulse intensity. For a fixed laser energy, the radiation intensity on the target can be increased or decreased by decreasing or increasing the focal spot size. It follows from our simulation results that the increase in the radiation intensity due to tight focusing is advantageous not only for increasing the maximum ion energy but also for increasing the number of ions, because thicker films can be used for acceleration in this case (Fig. 7b). In addition, tightly focused

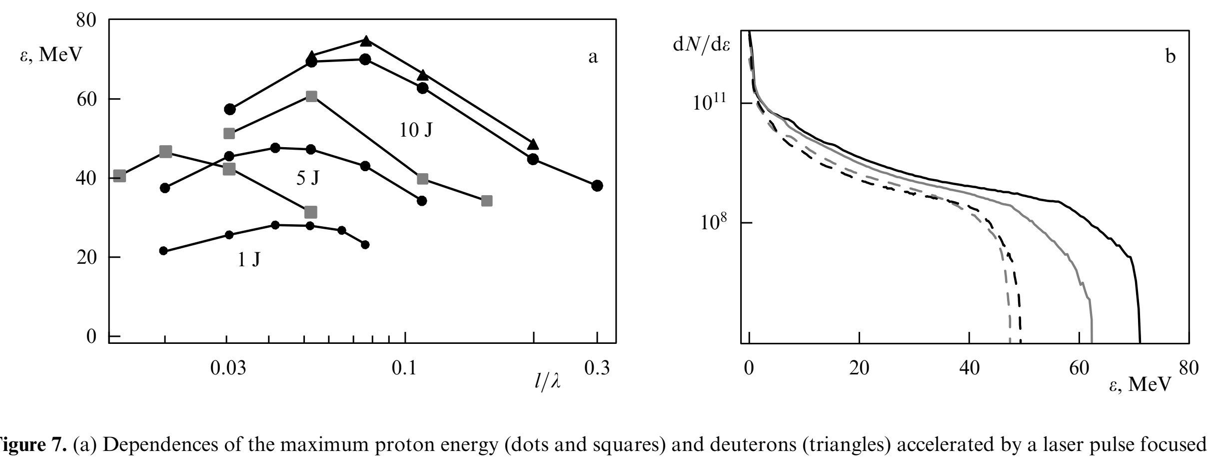

Figure 7. (a) Dependences of the maximum proton energy (dots and squares) and deuterons (triangles) accelerated by a laser pulse focused onto a spot 4 μm (circles and triangles), 6 μm (small squares), and 10 μm (large squares) in size on the target thickness for laser pulse energies of 10 J (large dots, squares, triangles), 5 J (medium-size dots), and 1 J (small dots). (b) Spectra of protons accelerated from targets with the optimal thickness irradiated by a 10 J laser pulse focused to a 4 μm spot (black solid curve), 6 μm spot (grey solid curve), and 10 μm spot (grey dashed curve), and a 5 J pulse focused to a 4 μm spot (black dashed curve).

laser pulses can produce approximately the same number of energetic particles as that produced by higher-power laser pulses focused onto a larger spot (cf. grey and black dashed curves in Fig. 7b).

Thus, by irradiating an optimal-thickness thin foil by a laser pulse, we can increase both the energy and number of accelerated protons. The laser-accelerated proton beam has a small angular spread ($\lesssim 10°$) and a broad energy spectrum with the maximum energy 50–70 MeV for a 10 J laser pulse. The number of accelerated protons with the energy exceeding 8 MeV is about 10^{11} per pulse.

Laser initiation of nuclear reactions involves the acceleration of ions (protons/deuterons) from a target irradiated by a laser pulse, followed by their interaction with a second nuclear target located behind. If we know the PIC-simulated spectrum of accelerated protons/deuterons, the reaction cross sections and energy losses during the propagation of particles through the target [40], and the decay constants of produced isotopes, the isotope yield can be estimated, for example, using the overlap integral [39]. The maximum yield of nuclear reaction products is analyzed below in the two examples of isotopes produced for medical applications (SPECT and PET).

We first estimate the Tc-99m yield (SPECT) obtained in the Mo-100(p, 2n)Tc-99m reaction initiated by a proton beam irradiating an enriched molybdenum target. The cross sections for various nuclear reactions in such interactions are well studied (see, e.g., [41]). The radioactivity A_0 of technetium isotopes after the 6-hour bombardment of a nuclear target by protons accelerated by a 10 kHz laser is presented in Fig. 8. We can see that the maximum radioactivity reaches ~ 0.5 TBq.

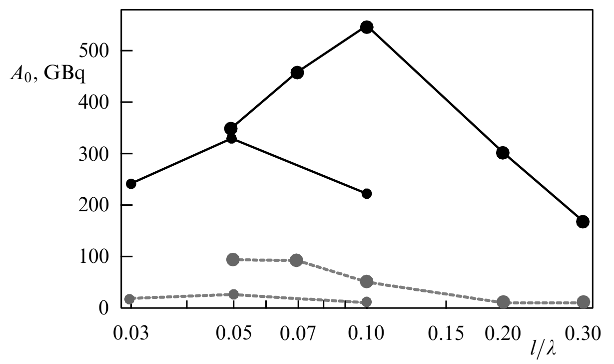

Figure. 8. Radioactivity of Tc-99m (black dots) and parasitic technetium isotopes (grey dots) after irradiation of an Mo-100 target by protons for 6 hours as a function of the laser target thickness irradiated by a 10 J laser (large dots) and a 5 J laser (small dots).

One of the main problems related to the Tc-99m quality obtained by this method is its radiative purity with respect to other technetium isotopes, which cannot be extracted from the final product by chemical methods. To achieve the radiative purity of the product, it is necessary to use a rather pure enriched molybdenum target (for example, ISOFLEX targets contain 99.54% of Mo-100, 0.41% of Mo-98, and only 0.05% of other quite hazardous impurities) and 40–45 MeV proton beams. Higher-energy protons, although producing a large amount of Tc-99m, give an unacceptably high level of other, parasitic radioactive technetium isotopes (first of all, Tc-96m). For a 63.5 MeV proton beam, the activity of parasitic technetium isotopes decreases from 7.5% immediately after the end of irradiation to 1.6% in the next three hours, whereas for a 46 MeV proton beam, the relative activity of parasitic technetium ions is only 0.12% after irradiation, decreasing to 0.03% in the next three hours. We note that these calculations neglect the activity of Tc-100 decaying into stable rubidium (with the decay time $\tau_{1/2} = 15.8$ s).

We now consider the production of a radioactive positron-emitting carbon C-11 isotope required for PET. This isotope can be produced in the 11B(p, n)11C reaction using a solid boron target and in the 14N(p, α)11C reaction using nitrogen gas targets. We also consider the possibility of using deuteron beams to irradiate an enriched boron-10 target for initiating the 10B(d, n)11C reaction (Fig. 9). For the particles of a sufficiently high energy considered above, the 11B(p, n)11C reaction is the most advantageous, being capable of producing 6.3×10^8 C-11 atoms using a 0.07 μm thick laser target to obtain a proton beam. This result qualitatively coincides with the estimate in [42] based on two-dimensional simulation, but allows a more accurate quantitative estimate of the product yield.

The neutron yield obtained in various reactions can be estimated similarly. For example, the total number of deuterons with the energy above 1 MeV produced in the 7Li(d, n)8Be reaction by irradiating a 0.07 μm thick CD_2 target with a 10 J laser pulse is 4×10^{11}, providing the production of 2.2×10^9 neutrons (Fig. 9b). By increasing the

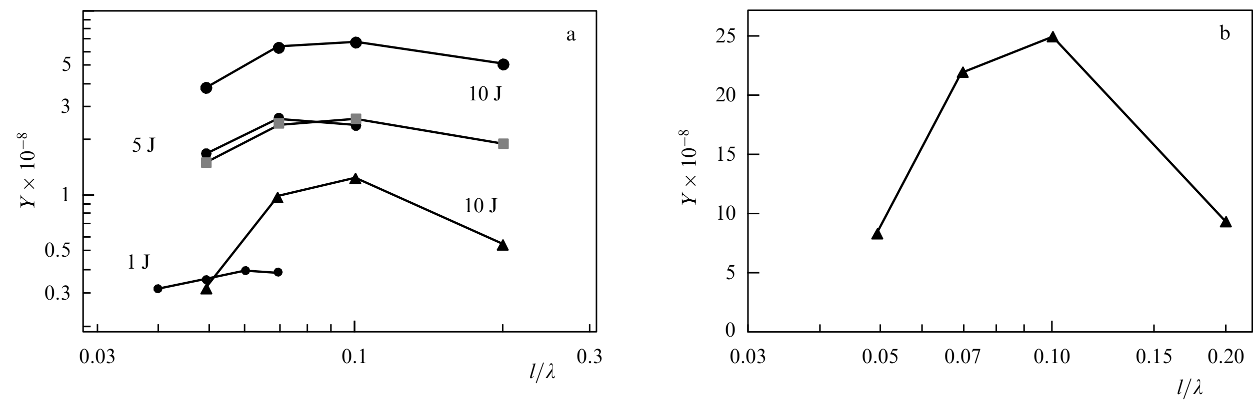

Figure 9. (a) Dependences of the C-11 isotope yield in 11B(p, n)11C (dots), 14N(p, α)11C (squares), and 10B(d, n)11C (triangles) reactions on the thickness of a laser target irradiated by a 10 J (large dots, triangles, squares), 5 J (medium-size dots), and 1 J (small dots) laser to obtain proton/deuteron beams. (b) The neutron yield in the 7Li(d, n)8Be reaction as a function of the thickness of a laser target irradiated by a 10 J laser.

laser target thickness to 0.1 μm, it is possible to accelerate up to 4.7×10^{11} deuterons, resulting in an increase in the neutron yield to 2.5×10^{9}. These values are in qualitative agreement with the results of two-dimensional calculations [43] predicting the neutron yield of 10^{8} sr per J of laser energy.

Thus, a 10 kHz, 10 J laser can generate a neutron flux containing $\sim 10^{13}$ s^{-1} particles, which considerably exceeds the neutron flux from neutron tubes. Such a setup produces about 2 TBq of activity of the C-11 isotope for 10 min of continuous irradiation and about 300 GBq of activity of the Tc-99m isotope for 6 hours, which is sufficient for medical purposes.

5. Analytic approaches

As an alternative to the planar targets considered in Section 4, a rarefied medium such as a gas plasma or a cluster plasma, which are the simplest targets for lasers with high pulse repetition rates, have long been discussed. The potential of such targets for obtaining high currents of accelerated ions is not yet fully realized, but a number of interesting features of the acceleration of particles that could be used are already evident. Here, we consider two examples illustrating this with analytic approaches.

5.1 Relativistic Coulomb explosion of a spherical microplasma

We demonstrate the possibility of studying the physics of ion acceleration with the example of an exact analytic solution [44] of the Coulomb explosion problem for a homogeneous spherical microtarget (cluster) providing a relativistic acceleration of ions upon its irradiation by a femtosecond laser pulse. Because the laser pulse is short, it must satisfy the only requirement, that its intensity be high enough to provide the rapid removal of electrons from the target in the course of the pulse duration, thereby producing a charged plasma almost instantly. The initial equations are the Poisson equation and the equations of cold collisionless hydrodynamics for the density $n_{\rm i}$ and the ion velocity u. The solution of these equations for an initially homogeneous cluster with the radius r_0 and density n_0 can be written in a parametric form as

$$\begin{aligned}
&u=\frac{2qc\sqrt{\zeta(1+q^2\zeta)}}{1+2q^2\zeta}\,,\quad r=\frac{h}{1-q^2}\,,\quad 0\leqslant h\leqslant r_0\,,\\
&n_{\rm i}=n_0\,\frac{(1-q^2)^3}{A}\,,\quad \zeta=\frac{\omega_{\rm pi}^2h^2}{6c^2}\,,\\
&A=1-\frac{q^2\zeta(1+\zeta)^{-2}}{1+2\zeta q^2}\left[3+5\zeta q^2+2\zeta^2q^2\right.\\
&\qquad\left.+\frac{3(1-q^2)\sqrt{1+\zeta q^2}}{2q\sqrt{1+\zeta}}\ln\frac{\sqrt{1+q^2\zeta}-q\sqrt{1+\zeta}}{\sqrt{1+q^2\zeta}+q\sqrt{1+\zeta}}\right],\\
&\sqrt{\frac{2}{3}}\,\omega_{\rm pi}t=\frac{q}{1-q^2}\sqrt{1+q^2\zeta}\,\frac{1+2\zeta}{1+\zeta}\\
&\qquad-\frac{1}{2}(1+\zeta)^{-3/2}\ln\frac{\sqrt{1+q^2\zeta}-q\sqrt{1+\zeta}}{\sqrt{1+q^2\zeta}+q\sqrt{1+\zeta}}\,,
\end{aligned}\tag{5}$$

where $\omega_{\rm pi}=(4\pi Z^2e^2n_0/M)^{1/2}$ is the Langmuir ion frequency. The solution in (5) describes an expanding ion bunch with the sharp front $r_{\rm f}(t)$. For a sufficiently large cluster charge, when the condition $\zeta(h=r_0)\equiv\zeta_0=\omega_{\rm pi}^2r_0^2/6c^2>1$ is satisfied, the accelerated ions, at least near the cluster boundary, can reach relativistic energies. The electric field, the ion velocity, and the density are maximal at the ion front of the relativistic cluster flying apart. The ion-front law of motion is determined by the expression $r_{\rm f}=r_0/(1-q_0^2)$. The relation between t and q_0 is

$$\sqrt{\frac{2}{3}}\,\omega_{\rm pi}t=\frac{q_0}{1-q_0^2}\sqrt{1+q_0^2\zeta_0}\,\frac{1+2\zeta_0}{1+\zeta_0}-\frac{1}{2}(1+\zeta_0)^{-3/2}\ln\frac{\sqrt{1+q_0^2\zeta_0}-q_0\sqrt{1+\zeta_0}}{\sqrt{1+q_0^2\zeta_0}+q_0\sqrt{1+\zeta_0}}\,.$$

In the nonrelativistic limit $\zeta_0\to0$, this solution reproduces the well-known result [45, 46] that the velocity of ions emitted from a homogeneous spherical target and the electric field inside the cluster linearly increase with increasing the coordinate r, attaining a maximum at the front $r=r_{\rm f}$. The ion density distribution in the cluster preserves its initial shape of a 'step' with varying width and height. The front propagation velocity $u_{\rm f}=\dot r_{\rm f}$ increases with time as $u_{\rm f}=\sqrt{(2/3)\,\omega_{\rm pi}r_0(1-r_0/r_{\rm f})}$, tending to the limit maximum value $u_{\rm m}=\sqrt{2/3}\omega_{\rm pi}r_0$. Correspondingly, the maximum energy of accelerated ions is $\varepsilon_{\rm m}=M(\omega_{\rm pi}^2r_0^2/3)$.

Passing to the relativistic limit $\zeta_0>1$ changes the shape of the ion velocity, density, and electric field spatial distributions: the ion velocity increases more slowly with increasing the distance from the cluster center, and, vice versa, the electric field inside the cluster increases faster for large radii and more slowly for small ones. The electric field outside the cluster decreases as $\sim r^{-2}$. As regards the ion density distribution, it becomes inhomogeneous along the radius with time and reaches its maximum at the front of cluster ions flying apart. Thus, the relativistic regime of the Coulomb explosion of the cluster is characterized by the formation of the peripheral densification of the plasma, i.e., a distribution of the envelope type, as shown in Fig. 10a. According to (5), the ion energy $\varepsilon=2Mc^2q^2\zeta$ becomes relativistic when $q^2\zeta$ is of the order of unity, which corresponds to the time $t_h\approx\sqrt2h/(c\zeta)$. In particular, setting $h=r_0$ and $\zeta=\zeta_0$ for ions at the front, we obtain $t_{r_0}\approx\sqrt2r_0/(c\zeta_0)$. We note that, asymptotically as $t\to\infty$, the maximum ion energy at the front is determined by the same expression $\varepsilon_{\rm m}=M(\omega_{\rm pi}^2r_0^2/3)$, as in the nonrelativistic case. The expression for the spectral distribution of accelerated cluster ions $N_\varepsilon\equiv{\rm d}N/{\rm d}\varepsilon$, taking (5) into account, has the form

$$N_\varepsilon=\frac{3h}{2Z^2e^2q^2}\left[1+\frac{1-q^2}{2q^2}\,(A-1)\right]^{-1}.\tag{6}$$

Here, the quantities h and q should be expressed in terms of ε with the help of the implicit relation $\varepsilon=2Mc^2q^2\zeta$ and the last equation of system (5). After integration over energy, quantity (6) coincides with the total number of particles in the cluster $N_0=(4\pi/3)\,n_0r_0^3$. Expression (6) gives the simple asymptotic relation

$$N_\varepsilon\big|_{t\to\infty}=\frac{3N_0}{2\varepsilon_{\rm m}^{3/2}}\sqrt{\varepsilon}\tag{7}$$

for the energy spectrum of ions. The absence of the dependence on the speed of light in (7) means that the spectral distributions of ions in relativistic and nonrelativistic cases asymptotically coincide. This statement is illustrated by the energy spectra of ions at different instants in Fig. 10b, which shows how the spectral distribution of ions gradually

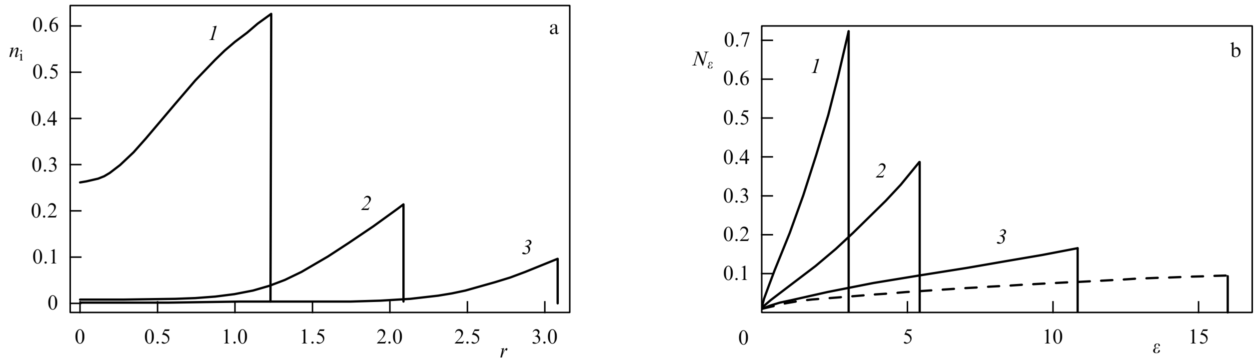

Figure 10. Spatial distribution of (a) the ion density and (b) the energy ion spectrum for instants of time $\omega_{\mathrm{pi}}t = 2$ (curves *1*), $\omega_{\mathrm{pi}}t = 8$ (curves *2*), and $\omega_{\mathrm{pi}}t = 15$ (curves *3*) for $\zeta_0 = 8$. The dashed line in Fig. b shows the spectrum for $\omega_{\mathrm{pi}}t \to \infty$. The ion density n_i is normalized to n_0, the spectral energy density N_ε is normalized to N_0/Mc^2, the radius r is normalized to r_0, and the energy ε is normalized to Mc^2.

flattens, approaching the $\sqrt{\varepsilon}$ profile with time. The dashed line in Fig. 10b corresponds to the asymptotic spectrum of ions in Eqn (7).

The physics of a relativistic Coulomb explosion is important for understanding how ions fly apart from targets with a complex ion composition. Of special interest is the Coulomb explosion of a quasi-homogeneous spherical target consisting of light and heavy ions [47]. The light ions fly apart faster, and although they were initially distributed homogeneously, they are found to be on the target periphery and are efficiently accelerated by the Coulomb field of heavy ions following behind them, which acts as a Coulomb piston and can produce a distinct cluster (in the form of an envelope) consisting of almost monoenergetic light ions like those predicted in the Coulomb explosion of spherical clusters with an envelope consisting of light ions [48]. The possibility of obtaining the higher energy per nucleon and, especially, the monochromatic spectrum of light ions is attracting attention to the study of the Coulomb explosion of a quasi-homogeneous plasma microdrop with a complex ion composition [47]. Analytic calculations for laser-produced sources of light ions show how the relativism of the Coulomb explosion determined by the total charge of the cluster affects the spectral characteristics of accelerated particles. In the nonrelativistic case, the accelerated impurity of light ions has good monochromaticity [47], but the spectral distribution of ions broadens in passing to the strongly relativistic explosion regime. However, impurity ions with the relativistic energy can appear even for a 'moderate' cluster charge, when the 'relativism parameter' ζ_0 is smaller than unity. In this case, the maximum energy of impurity ions becomes higher than in the nonrelativistic limit, and the characteristic width of the spectrum of accelerated ions is comparable with that in the nonrelativistic limit.

5.2 Radial acceleration of ions by a laser pulse in a plasma channel

Another illustration of the application of theoretical methods is an analytic solution of the problem of radial acceleration of particles from a laser channel (rarefied gas plasma [49, 50] or plasmas in new-generation low-density targets such as aerogels or porous nanocarbon). The analytic description of the acceleration of particles from a plasma channel formed due to self-focusing is not a simple problem even for approximate approaches. For this reason, the space–time distribution of accelerated particles is typically studied using kinetic numerical PIC simulations. A certain simplification is introduced by a one-dimensional electrostatic ponderomotive model describing the dynamics of plasma expansion caused by pulsed laser irradiation with the specified intensity distribution along the plasma channel radius [49, 50]. The model considers only the slow dynamics of plasma electrons, which corresponds to averaging over fast electron oscillations in the laser field. Although such a description is simplified, the main results obtained for the electrostatic ponderomotive model are also based on numerical PIC simulations, complicating the prediction of characteristics of accelerated particles as functions of laser and plasma parameters. Numerical simulations [49, 50] have revealed two distinct effects: (i) the formation of a cylindrical density cusp at the laser channel boundary due to the acceleration of ions by the ponderomotive force and (ii) the strong local heating of electrons at the laser channel boundary.

The group theory approach based on the use of renormalization-group (RG) symmetries [51] is an efficient tool for the analytic solution of problems on laser–plasma acceleration of charged particles [29, 52]. The kinetic equation for an electron averaged over fast laser oscillations in the model of radial ponderomotive acceleration of particles from the laser channel includes an 'external' electric field specifying the radial ponderomotive force acting on plasma electrons [53] in addition to the self-consistent electric field of plasma. The particle acceleration dynamics can be described by kinetic equations for the distribution functions of plasma particles integrated over the longitudinal and axial velocity components (electrons, $f_\mathrm{e} = (n_{\mathrm{e}0}/V_{\mathrm{Te}})\, g(\tau, x, u)$, and ions, $f_\mathrm{i} = (n_{\mathrm{e}0}/(Zc_\mathrm{s}))\, f(\tau, x, w))$ and the Poisson equation $E = (T_{\mathrm{e}0}/\varepsilon e L)\, p(\tau, x)$ for the electric field. Here, $\tau = \omega_{\mathrm{pi}}t$ is the dimensionless time, with ω_{pi} being the ion Langmuir frequency; $x = r/L$ is the dimensionless coordinate, where L is the localization scale of the laser beam along the radius; $u = v_r^\mathrm{e}/V_{\mathrm{Te}}$ is the electron velocity, with $V_{\mathrm{Te}} = \sqrt{T_{\mathrm{e}0}/m}$; $w = v_r^\mathrm{i}/c_\mathrm{s}$ is the ion velocity, with $c_\mathrm{s} = \sqrt{ZT_{\mathrm{e}0}/M}$, and m and M being the respective electron and ion mass; $e_\mathrm{e} = -e$ and $e_\mathrm{i} = Ze$ are the respective electron and ion charges, where Z is the charge number of ions.

The initial particle distribution functions are assumed to be Maxwellian with a homogeneous initial electron and ion temperatures $T_{(\mathrm{e,i})\,0}$ and initial densities $n_{(\mathrm{e,i})\,0}(x)$ with a characteristic spatial scale L that considerably exceeds the Debye electron radius $\lambda_{\mathrm{De}} = \sqrt{T_{\mathrm{e}0}/(4\pi n_{\mathrm{e}0} e^2)}$, i.e., $\varepsilon = \lambda_{\mathrm{De}}/L \ll 1$. We note that specifying a finite initial temperature of particles corresponds to the physical setup of the problem, because a propagating high-power laser pulse is typically preceded by a long prepulse that heats the plasma by the time of the arrival of the main pulse. An approximate analytic solution of kinetic equations for the distribution functions of particles with zero mean velocities has the form

$$
\begin{aligned}
f &= \frac{x' n_{i0}(x')}{x\sqrt{2\pi}\Gamma} \exp\left[-\frac{(\zeta'-q')^2(w-W)^2}{2(\zeta-q)^2\Gamma^2}\right],\\
p &= -q - \varepsilon\,\frac{(\zeta'-q')^3}{(\zeta-q)^3}\,\frac{\partial_{x'}(n_{e0}(x'))}{n_{e0}(x')},\\
g &= \frac{x' n_{e0}(x')}{x\sqrt{2\pi}} \exp\left[-\frac{(\zeta'-q')^2(u-U)^2}{2(\zeta-q)^2}\right],\\
\zeta(x) &= -\varepsilon\left(\frac{\partial_x n_{e0}}{n_{e0}} + \Gamma^2\,\frac{\partial_x n_{i0}}{n_{i0}}\right), \quad \Gamma^2 = \frac{T_{i0}}{ZT_{e0}},
\end{aligned} \tag{8}
$$

where

$$
\begin{aligned}
W = &-\frac{1}{3}(4q-\zeta)(\zeta-q)\sqrt{\frac{Z(y)}{2}}\\
&+\frac{1}{2(\zeta-q)}\int_{y'}^{y}\mathrm{d}\xi\left[\frac{1}{3}\sqrt{\frac{2}{Z(\xi)}}-\sqrt{2Z(\xi)}\zeta(\zeta-q)\,\partial_\xi(\zeta-q)\right.\\
&\left.+\frac{\zeta}{\left(\sqrt{2Z(\xi)}\,(\zeta-q)\right)}\right], \quad U = \mu W, \quad \mu = \sqrt{\frac{Zm}{M}},
\end{aligned} \tag{9}
$$

and the variable x' is expressed in terms of τ and x as

$$
\begin{aligned}
&\frac{\tau^2}{2(\zeta-q)^2} - Z(y) = -Z(y'),\\
&Z(y) = \int_{y'}^{y}\frac{\mathrm{d}\xi}{\left(\zeta(\xi)-q(\xi)\right)^3}, \quad y = \frac{x}{\varepsilon}.
\end{aligned} \tag{10}
$$

Here, $q = \alpha\partial_x\gamma$, where $\alpha = \varepsilon(c^2/V_{Te}^2)$, c is the speed of light, $\gamma = (1 + a^2(\tau,x)/2)^{1/2}$, and $a^2(\tau,x) = A(\tau)\,a_0^2 I_0(x)$ is the dimensionless laser intensity, where $A(\tau)$ is the laser pulse shape. The function $I_0(x)$ is the radial laser intensity distribution. For example, the function $I_0(x) = \exp(-x^2)$ was considered in [50]. Solution (8) corresponds to $A(\tau) = 1$, i.e., to a stationary (quasistationary) laser beam.

The global characteristics — the average velocity v_{av}^{i}, the density n_{av}^{i} of plasma ions, and the electron temperature T_e — can be calculated from the known particle distribution function (8) as

$$
\begin{aligned}
&v_{av}^{i} = W, \quad n_{av}^{i} = n_{i0}(x')\,\frac{x'(\zeta'-q')}{x(\zeta-q)},\\
&T_e = T_{e0}\,\frac{(\zeta'-q')^2}{(\zeta-q)^2}.
\end{aligned} \tag{11}
$$

Figure 11 shows spatial distributions of the mean ion density, the mean velocity of ions and the electron temperature at different instants for a stationary laser beam ($A(\tau) = 1$). The acceleration of ions is accompanied by the formation of an ion density cusp with a minimum at the laser beam center and a maximum at its periphery. A similar behavior is typical for the plasma electron temperature: T_e decreases in the central region of the laser beam and increases at its periphery. As τ increases, the conditions of the applicability of the theory based on the approximate symmetry are violated, and for $\tau \gtrsim 6$, the spatial distributions in Fig. 11 become only quantitative. In fact, the dashed curves in Fig. 11 for $\tau = 7$ reflect only a trend in the density and velocity of ions and the electron temperature, rather than their accurate values.

Thus, a significant achievement of the theoretical approach based on approximate RG symmetries is the possibility of describing not only the evolution of ions with the formation of an ion density cusp near the beam axis but also the inhomogeneous heating of electrons near the external boundary of the beam and their cooling in the near-axial region. These results theoretically explain the findings of numerical experiments [49, 50] and can be used to analyze the behavior of plasma particles at large times after the laser pulse is switched off. The model of a cylindrical laser channel proposed here corresponds to a $\gtrsim 100$ fs laser pulse focused onto a $\lesssim 10$ μm spot. For the laser intensity 10^{19}–10^{20} W cm^{-2}, the ponderomotive acceleration provides an increase in the proton energy to multimegaelectronvolts. Such ponderomotive-accelerated protons can initiate nuclear reactions [14] in the ambient gas or in a special coaxial with an appropriate atomic composition. This principle can be used for developing other laser sources of medical isotopes for PET or SPECT, different from those discussed in Section 4.

6. Conclusions

Despite a naturally low efficiency ($\ll 1$) of the laser pulse energy conversion to high-energy ions, the optimization of the laser–target system shows promise for reaching the parameters of accelerated ions required for nuclear applications after solving the highly technological problem of

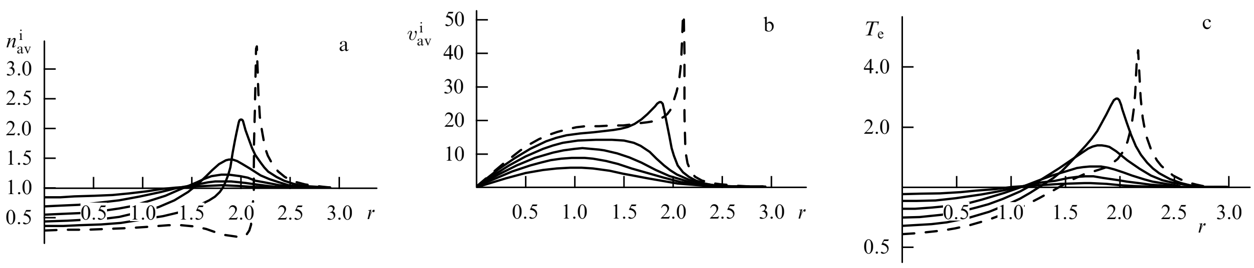

Figure 11. Spatial distributions of (a) the normalized average ion density n_{av}^{i}, (b) the normalized average ion velocity v_{av}^{i}, and (c) the electron temperature T_e over the dimensionless coordinate r for a stationary laser beam for $\tau = 2, 3, 4, 5, 6, 7$ (corresponding curves, from top down (for $r \to 0$) for n_{av}^{i} and T_e, and from bottom up for v_{av}^{i}) and for $Z = 2$, $A = 4$, $a_0^2 = 50$, $\alpha = 1$, $\varepsilon = 0.01$, $\mu = \sqrt{1/4000}$, $n_c/n_{e0} = 100$, $n_{e0} = 1$, $n_{i0} = 0.5$, and $\Gamma = 0.001$.

developing a femtosecond multijoule laser setup (like ICAN) with a kilohertz pulse repetition rate and a high pulse contrast on the picosecond scale. The obtained proton energy scaling $\varepsilon_{\max} \propto E_{\mathrm{L}}^{0.7}$ proves the possibility of using thin solid foils irradiated by such a laser for nuclear applications. At the same time, preliminary calculations show that it is necessary to initiate detailed studies of the ion parameters that can be achieved by using laser mechanisms of particle acceleration from low-density targets. Even if these parameters are only slightly improved, low-density targets may be advantageous because of their lower sensitivity to the laser pulse contrast. Here, the main practical goal is the development of nanoporous targets having a good homogeneity and a density comparable to the critical one.

Acknowledgments
Most of the studies considered in this paper were supported by the Russian Foundation for Basic Research (grants 12-02-00231, 13-02-00426, 14-02-31407-mol_a, 14-01-00828, and 14-29-09244-ofi_m) and grants from the President of the Russian Federation for the Support of Leading Scientific Schools (NSh-1424.2014.2, NSh-3003.2014.2) and part of the studies related to low-density targets is supported by the RSF grant No. 14-12-00194.

References

1. Gaillard S A et. al. *Phys. Plasmas* **18** 056710 (2011)
2. Snavely R A et al. *Phys. Rev. Lett.* **85** 2945 (2000)
3. Mackinnon A J et al. *Phys. Rev. Lett.* **88** 215006 (2002)
4. Fuchs J et al. *Nature Phys.* **2** 48 (2006)
5. Henig A et al. *Phys. Rev. Lett.* **103** 245003 (2009)
6. Lévy A et al. *Eur. Phys. J. Special Topics* **175** 111 (2009)
7. Dollar F et al. *Phys. Rev. Lett.* **108** 175005 (2012)
8. Vshivkov V A et al. *Phys. Plasmas* **5** 2727 (1998)
9. Esirkepov T, Yamagiwa M, Tajima T *Phys. Rev. Lett.* **96** 105001 (2006)
10. Brantov A V et al. *Phys. Rev. ST Accel. Beams* **18** 021301 (2015); arxiv:1409.3356
11. Bulanov S S et al. *Phys. Rev. E* **78** 026412 (2008)
12. Bychenkov V Yu et al. *Plasma Phys. Rep.* **27** 1017 (2001); *Fiz. Plazmy* **27** 1076 (2001)
13. Roth M et al. *Phys. Rev. Lett.* **86** 436 (2001)
14. Bychenkov V Yu, Tikhonchuk V T, Tolokonnikov S V *JETP* **88** 1137 (1999); *Zh. Eksp. Teor. Fiz.* **115** 2080 (1999)
15. Borghesi M et al. *Plasma Phys. Control. Fusion* **43** A267 (2001)
16. Mackinnon A J et al. *Rev. Sci. Instrum.* **75** 3531 (2004)
17. Nemoto K et al. *Appl. Phys. Lett.* **78** 595 (2001)
18. Bychenkov V Yu, Brantov A V, Mourou G *Laser Part. Beams* **32** 605 (2014)
19. Bulanov S V, Khoroshkov V S *Plasma Phys. Rep.* **28** 453 (2002); *Fiz. Plazmy* **28** 493 (2002)
20. Bychenkov V Yu, Brantov A V *Eur. Phys. J. Special Topics* **224** (2015), to appear
21. Mourou G et al. *Nature Photon.* **7** 258 (2013)
22. Korzhimanov A V et al. *Phys. Usp.* **54** 9 (2011); *Usp Fiz. Nauk* **181** 9 (2011)
23. Romanov D V et al. *Phys. Rev. Lett.* **93** 215004 (2004)
24. Brantov A, Bychenkov V Yu *Contrib. Plasma Phys.* **53** 731 (2013)
25. Govras E A, Bychenkov V Yu *JETP Lett.* **98** 70 (2013); *Pis'ma Zh. Eksp. Teor. Fiz.* **98** 78 (2013)
26. Mora P *Phys. Rev. Lett.* **90** 185002 (2003)
27. Bychenkov V Yu, Kovalev V F *Quantum Electron.* **35** 1143 (2005); *Kvantovaya Elektron.* **35** 1143 (2005)
28. Wilks S C et al. *Phys. Plasmas* **8** 542 (2001)
29. Kovalev V F, Bychenkov V Yu, Tikhonchuk V T *JETP* **95** 226 (2002); *Zh. Eksp. Teor. Fiz.* **122** 264 (2002)
30. Brantov A et al. *Contrib. Plasma Phys.* **53** 161 (2013)
31. Passoni M et al. *Plasma Phys. Control. Fusion* **56** 045001 (2014)
32. Korzhimanov A V et al. *JETP Lett.* **86** 577 (2007); *Pis'ma Zh. Eksp. Teor. Fiz.* **86** 662 (2007)
33. Bulanov S S et al. *Phys. Plasmas* **17** 043105 (2010)
34. Brantov A V, Bychenkov V Yu *Plasma Phys. Rep.* **40** 505 (2014); *Fiz. Plazmy* **40** 591 (2014)
35. Roth M et al. *Phys. Rev. Lett.* **110** 044802 (2013)
36. Van Noorden R *Nature* **504** 202 (2013)
37. Benard F et al. *J. Nucl. Med.* **55** 1017 (2014)
38. Bulanov S V et al. *Phys. Usp.* **57** 1149 (2014); *Usp. Fiz. Nauk* **184** 1265 (2014)
39. Krasnov N N *Int. J. Appl. Radiat. Isotop.* **25** 223 (1974)
40. Ziegler J F "Particle Interactions with Matter" (2010), http://www.srim.org/
41. Qaim S M et al. *Appl. Radiat. Isotop.* **85** 101 (2014)
42. Lefebvre E et al. *J. App. Phys.* **100** 113308 (2006)
43. Davis J et al. *Plasma Phys. Control. Fusion* **52** 045015 (2010)
44. Bychenkov V Yu, Kovalev V F *JETP Lett.* **94** 97 (2011); *Pis'ma Zh. Eksp. Teor. Fiz.* **94** 101 (2011)
45. Kaplan A E, Dubetsky B Y, Shkolnikov P L *Phys. Rev. Lett.* **91** 143401 (2003)
46. Bychenkov V Yu, Kovalev V F *Plasma Phys. Rep.* **31** 178 (2005); *Fiz. Plasmy* **31** 203 (2005)
47. Andriyash I A, Bychenkov V Yu, Kovalev V F *JETP Lett.* **87** 623 (2008); *Pis'ma Zh. Eksp. Teor. Fiz.* **87** 720 (2008)
48. Kovalev V F, Bychenkov V Yu, Mima K *Phys. Plasmas* **14** 103110 (2007)
49. Sarkisov S G et al. *Phys. Rev. E* **59** 7042 (1999)
50. Macchi A et al. *Plasma Phys. Control. Fusion* **51** 024005 (2009)
51. Kovalev V F, Shirkov D V *Phys. Usp.* **51** 815 (2008); *Usp. Fiz. Nauk* **178** 849 (2008)
52. Kovalev V F, Bychenkov V Yu *Phys. Rev. Lett.* **90** 185004 (2003)
53. Miller M A *Izv. Vyssh. Uchebn. Zaved. Radiofiz.* **1** 110 (1958)

PACS numbers: 41.75.Jv, **52.35.–g**, 52.38.Kd
DOI: 10.3367/UFNe.0185.201501g.0089

Plasma-based methods for electron acceleration: current status and prospects

I Yu Kostyukov, A M Pukhov

Abstract. **We present a short review of the current status of plasma-based methods for electron acceleration. Plasma acceleration mechanisms are described, with an emphasis on the most important experimental results and theoretical models. Some new areas of research in plasma-based methods are discussed. We also analyze future prospects for plasma accelerators and their usage in electromagnetic radiation sources of high-intensity.**

Keywords: laser-plasma acceleration methods, laser pulse, electron beam, self-injection.

1. Introduction

Charged particle accelerators are one of the most important inventions of the 20th century. At the present time, accelerators are extremely important tools in the field of high-

I Y Kostyukov Institute of Applied Physics of the Russian Academy of Sciences, Nizhny Novgorod, Russian Federation;
Lobachevsky State University of Nizhny Novgorod, Nizhny Novgorod, Russian Federation
E-mail: kost@appl.sci-nnov.ru
A M Pukhov Heinrich-Heine Universität Düsseldorf, Düsseldorf, Deutschland; Lobachevsky State University of Nizhny Novgorod, Nizhny Novgorod, Russian Federation

Uspekhi Fizicheskikh Nauk **185** (1) 89–96 (2015)
DOI: 10.3367/UFNr.0185.201501g.0089
Translated by A L Chekhov; edited by A Radzig